Challenges and limits of Mechanical Stability in 3D Direct Laser Writing

Elaheh Sedghamiz
Karlsruhe Institute of Technology
Modan Liu
Karlsruhe Institute of Technology
Wolfgang Wenzel (wolfgang.wenzel@kit.edu)
Karlsruhe Institute of Technology https://orcid.org/0000-0001-9487-4689

Article

Keywords: direct laser writing, mechanical stability

Posted Date: February 1st, 2021

DOI: https://doi.org/10.21203/rs.3.rs-151096/v1

Version of Record: A version of this preprint was published at Nature Communications on April 19th, 2022. See the published version at https://doi.org/10.1038/s41467-022-29749-9.

Challenges and limits of Mechanical Stability in 3D Direct Laser Writing

Elaheh Sedghamiz, Modan Liu and Wolfgang Wenzel*

Institute of Nanotechnology (INT), Hermann-von-Helmholtz-Platz 1, 76344 Eggenstein-Leopoldshafen, Karlsruhe Institute of Technology (KIT), Germany.
E-mail: wolfgang.wenzel@kit.edu

Abstract

Direct laser writing is an effective technique for fabrication of complex polymeric 3D polymer networks using ultrashort laser pulses. Practically, it remains a challenge to design and fabricate high performance materials with different functions that possess a combination of high strength, substantial ductility, and tailored functionality, in particular for small feature sizes. To date, it is difficult to obtain a time-resolved microscopic picture of the printing process in operando. To close this gap, we herewith present a molecular dynamics simulation approach to model direct laser writing and investigate the effect of writing condition and aspect ratio on the mechanical properties of the printed polymer network. We show that writing condition provides a possibility to tune the mechanical properties and an optimum writing condition can be applied to fabricate structures with improved mechanical properties. We reveal that beyond the writing parameters, aspect ratio plays an important role to tune the stiffness of the printed structures.

Introduction

Three-dimensional direct laser writing (3D-DLW) is an indispensable tool for high accuracy structuring and fabricating of arbitrary 3D micro- and nano-objects via a non-linear absorption induced polymerization process [1–3]. Over the past decade, this technology has become a well-established lithography tool for fabricating a wide variety of 3D structures directly on functional substrates [4,5]. This technique enabled a wide range of applications in photonics [6], microfluidics [7], as well as the generation of mechanical microstructures [8], and cell scaffolds [9]. Despite recent advances in the manufacturing techniques and its applications, different limitations and challenges remain. For example, new photoresist formulations for fabricating conducting polymer devices [10,11], integrating new biocompatible materials [12], the integration of multiple materials in the same structure [13], increasing the structuring rate [14,15], and obtaining sufficient and controllable stiffness of the fabricated structure [16,17]. Moreover, the relatively large feature size and limited resolution of DLW compared to electron-beam lithography (EBL) and focused ion beam milling have limited its application to deep sub-micron lithography. Several strategies have been applied in order to decrease feature size driven by interest in shrinking devices to nanometer scales, such as, introducing mobile quenching molecules [18] and implementing a second annular inhibiting laser, *i.e.* stimulated emission depletion (STED) lithography [19]. To the best of our knowledge, the smallest feature size and the separation achieved to date are 7 and 33 nm, respectively [20].

Recently, there has been a growing effort to bring direct laser fabrication from a laboratory curiosity to a versatile tool for the fabrication of various micro- nano-structures of 3D materials for functional devices [21–23]. It has been observed that, while fabricating structures with higher stiffness is favorable in many applications [11], in some applications, such as tissue engineering, 3D scaffolds with smaller Young's modulus result in a better functionality as compared to stiffer structures [24]. In addition, structural modifications induced by shrinkage or insufficient stability during drying must be considered in the development step [25,26]. Overall, the morphology and

stiffness of the fabricated micro-/nano-structure play a key role in the functionality of the structure [13,16] and it is important to understand how both parameters can be controlled in the context of the DLW process parameters. This is of particular relevance for improved manufacturing of delicate structures. Experimental studies in this realm encounter serious challenges as it is not easy to control all parameters that influence the DLW process [27] or to observe this process on the nanoscale *in operando*. Additionally, difficulties in reliable fabrication of nanoscale specimens in combination with strain measurement complications make mechanical experiments challenging [28].

To complement the experiment, computer simulations offer a time-resolved virtual analogue of the 3D writing process, in particular at small scales and promise insights into the details of this process that are difficult to obtain by experiment. Given its favorable cost, simulations allow for systematic studies of the variation of structure and stiffness of the fabricated polymer network [29,30] as a function of the process and materials parameters, which – in the long term – potentially enables virtual design/screening of materials and process conditions. There have been several studies attempting to emulate the two-photon polymerization conditions and extract the role of various involved process and material-dependent parameters [31–33]. Analytical models have been developed that model termination via radical combination and radical trapping to investigate the effect of photoinitator concentration, light intensity and oxygen quenching on the polymerization process and time dependent conversion [31–33]. While these numerical models are able to capture some aspects of laser-induced polymerization, their limitation is the lack of molecular scale information and parameters that must be fitted to experiment. This limits the long-term potential of these methods and their predictive value.

With the continuous improvement of computational resources, molecular dynamics (MD) simulation, which represent both the molecular structure of the system and the dynamics of the process, has emerged as an increasingly powerful tool to model complex structure formation processes. This approach is capable to model many process parameters and yields structural

models that can be analyzed with respect to their mechanical properties [34–37] but remains limited with respect to system size and the time scales that can be treated [30,38,39]. To date, there have been few studies that systematically investigated the influence of the initial composition and process parameters on the formation of the polymer network and its properties. Wang et. al [40] have used this approach in order to model continuous liquid interface production (CLIP) 3D printing technique aiming to investigate the effects of elastic, capillary and friction forces on the quality of the shape of the 3D printed objects. Nevertheless, the accurate correlation between the writing condition, architecture and mechanical properties of the printed structures in DLW remains elusive and no theoretical model has been developed to dispel this issue.

In this work, we develop and apply a molecular dynamics (MD) based protocol to simulate direct laser writing of 3D polymer networks starting from acrylate-based monomers, where monomers stick irreversibly with respect to experimental reaction rate constants by focusing on an experimentally important system. We employ a coarse grained MD simulation approach to explore the mechanical stability of 3D printed polymer networks of different aspect ratios applying different laser powers and exposure times and to explain how the structural and mechanical properties of the printed polymer network are correlated to DLW condition and their aspect ratio.

Results and discussions

Characterization of the printed polymer networks

The degree of monomer conversion i.e. the fraction of bound functional groups as compared to the overall number of functional groups is an important parameter for polymerization reactions, especially in the DLW process. In polymer chemistry, it has been found that there is a saturation for monomer conversion as a function of the reaction time [41]. In the case of DLW, different authors reported different degrees of conversion for commercial and non-commercial photoresists [41,42]. While the control of the degree of polymerization in the voxel during the

actual writing process is of utmost importance for further improvements of DLW, it has been a challenge to directly measure the level of chemical conversion in the printed area. A few studies investigate the effect of the writing condition on the properties of the printed polymer network [28,42–46]. By using different detection instrumentations, for non-commercial resists based on a mixture of two different tri-acrylates, a monomer conversion degree of 60%-75% has been obtained while for organic-inorganic hybrid resists, degree of conversion has been reported to be 35%-75% [42,43]. Nevertheless, it is clear that solidification and formation of chemically stable networks occurs at relatively low conversions well below 100%.

We first consider different scenarios for the polymerization time vs. the exposure time, the former being defined as the time where a substantial polymerization can be observed, even after no new free radicals are generated anymore. To illustrate this effect, Fig. 2 shows the kinetics of monomer consumption in one voxel for two different exposure times, *i.e.* 50 and 500 time steps. For the short exposure time, the polymerization reaction occurs from 0 to 200 τ while for the longer exposure time it occurs between 0 to 170 τ. For the simulation with a exposure time of 50 τ, a significant amount of polymerization occurs after the exposure (dark polymerization) which is the common scenario in DLW of all tri-acrylate based photoresists [33]. We note that in this scenario, some free monomers are left within the exposure area while for long exposure times, all monomers are being consumed during the exposure time.

To systematically study the degree of monomer conversion as a function of laser power and different exposure times, we fabricated a cubic polymer network of size 40×40×40 σ with an initial volume fraction of 85% monomers. As expected, the conversion increases with higher laser power or, correspondingly, higher exposure times and saturates towards high writing powers as shown in Fig. 2. We find that the laser power has a stronger influence on the degree of monomer conversion than the exposure time. For instance, increasing the laser power from 23 to 45 mW increases the degree of conversion from 69% to 77%, while at the subsequent increments to 65 mW, the degree of monomer conversion only increases by ~2 percentage

points. Hence, it is sufficient to apply moderate laser powers of 40-45 mW to reach a high monomer conversion ratio.

In addition, Fig. 2 shows that the exposure time has a more pronounced effect on monomer conversion at lower laser powers. These findings are in good agreement with the experimental results obtained by Cicha et al. [42] on tri-acrylate based photoresists.

Having generated a number of protocols for different exposure conditions, we are now able to characterize the mechanical properties of the polymerized network. It has been found that the laser power applied for photo-polymerization critically affects mechanical properties of the final structure [17]. To study the mechanical properties, we fabricate cubic polymer networks applying different laser powers and constant writing velocities. We find that the increase of laser power leads to the higher cross-linking density (number of the monomers that formed the maximal 3 bonds in this case) as shown in Fig. 3 (A-C). The degree of monomer conversion is increasing from 65% to 77% for the applied laser powers, as illustrated in Fig. 3 (D).

The mechanical properties of the printed networks are studied by simulating stress-strain dependencies and calculating the Young's modulus (E) from the slope of the stress–strain curve under different writing conditions, as discussed in the methods section. As shown in Fig. 3 (D), stress increases by increasing the laser power which is consistent with the behavior of the tri-acrylate photoresist under similar conditions [17,28]. Stress-strain curves do not illustrate a linear elastic behavior but they show a degree of hyperelasticity which is the typical behavior of rubbery materials under the mechanical test reflecting a two-region behavior (linear and nonlinear) [47]. The first region, between 0 and 0.5, with the smaller slope corresponds to the increase of the stress due to the recoiling of the polymer chains and the part with the larger slope corresponds to the FENE bond stretching which is schematically shown in the insets of Fig. 3 (D) [17,48]. Mechanical properties of the printed networks can be better quantified by estimating E from the slope of the stress-strain curve (Fig. 3 (E)). We find that for laser powers below 35 mW, E increases linearly as a function of the laser power and reaches a threshold for

higher laser powers. Lemma et. al.[17] performed a linear fit of E values obtained for laser powers below 20 mW, however, it was not possible to obtain experimental data for higher laser powers as overheating causes damage of the polymerized structure at high laser powers [41]. Therefore, Fig. 3 (E) suggests that a polymer network with near-maximal stiffness can be obtained by applying the moderate laser powers between 35 mW to 40 mW. Our simulation shows that applying such laser power results in polymer network with ~70% degree of monomer conversion (degree of monomer conversion is increasing from 61% for the lowest laser power to 73% for the highest one).

Effect of writing velocity on the properties of printed polymer networks

Mechanical properties of printed objects needs tuning to enhance the performance in some applications. For instance in the field of tissue engineering, the Young's modulus of the synthesized scaffold must vary for different kinds of the cells to regenerate better [16,49–51]. One direct approach for modifying the modulus is to change the writing laser power as we illustrated earlier. However, in experiment, sometimes it is easier to change the writing velocity rather than the laser power during the polymerization [52]. To investigate the effect of writing velocity on the mechanical properties of the printed objects, we fabricate cubic polymer networks by applying different exposure times (different writing velocities) and constant laser power. Therefore, the decrease in the exposure time leads to decrease in the number of active monomers and lower cross-linking density. Then we deform the fabricated networks to obtain the stress-strain curve and calculate the Young's Modulus using the same procedure as explained in the previous section. As shown in Fig. 4, the Young's modulus increases with the exposure time, which is the direct result of increasing the degree of monomer conversion, which increases from 59% for t=200τ, to 63% for t=400τ, to 65% for t=800τ and 66% for t=1200 τ. The Young's modulus increases by about 50% (from ~1 ε/σ^3 to ~1.5 ε/σ^3) by increasing the exposure time from 200 τ to 1200 τ. It reaches a threshold value at $\tau = 1200$ which indicates the saturation in cross-

linking density. It is due to the fact that all activated monomers polymerize in the early stage of the exposure time and further exposure leads to an increase in cross-linking density, however, in longer exposure times, the high steric effect within the formed 3D network do not allow for further cross-linking between the polymer chains.

Stiffness of the printed polymer rods

Recent developments in nano-scale devices take advantage of many complex patterns with high aspect ratio structures in its design [45,53–56]. High strength along with high deformability is an essential property for the design and reliability of novel nano devices [57]. The stress-strain curves, which result from a collective effect from all the particles, do not depend on the aspect ratio of the structure.

To investigate the stiffness and deformability of small printed objects, we are more interested in some local events to understand how polymer networks of different aspect ratios behave under an external loading force as these local events can lead to crack formation. Therefore, nano-rods with different aspect ratios (length to diameter ratio) i.e. 20 σ, 30 σ, 40 σ and 50 σ cross section diameter and 120σ height were fabricated (see Fig. 5) in a monomer pool of 80σ×80σ×240σ applying different laser powers ranging from 10 to 50 mW.

The printed rods were deformed under the influence of an external force (details are provided in the method section). The maximum amount of the deflection versus the cross-section diameter for different laser powers are shown in Fig. 6. It shows that the deflection is decreasing as the cross-section diameter is increasing for all applied laser powers, which indicates that printed objects with higher aspect ratios have lower stiffness and hence higher flexibility (deformability). Nevertheless, it is also important to investigate the probability of crack formation for each rod in the deformation test.

To understand how the printed samples behave under an external force, we investigate some local properties, *i.e.* particle strain inside the rods at their maximum deformation. In Fig. 7, we

plot the distribution of atomic strains for all fabricated samples at their maximum deflection. All microstructural analysis and visualization of atomic strains are performed using the open-source visualization tool OVITO [58]. The highly localized, high-strain region are observed for all samples with high aspect ratios $w/h = 6$ and 4 which get smaller by increasing the laser power. This region of high strain in high aspect ratio structure is likely to yield the onset of a fracture for all applied laser powers. Note, in our simulations the actual formation of a fracture cannot be observed since the structures are small and our model does not implement bond breaking. For samples with $h/w = 3$, large areas of moderate atomic strain along with small regions of high strain is observed at low laser powers which disappear by increasing the laser power. For samples with $h/w = 2.2$, no high strain region can be detected, instead there exist low to moderate strain regions spreading throughout the deformed areas. Furthermore, no significant difference in the strength and distribution of atomic strain can be seen for structures with smaller aspect ratios.

Therefore, the stiffness of high aspect ratio rods are largely independent on the applied writing condition i.e. laser power, suggesting the existence of a size threshold for which the expected writing condition-sensitivity does not apply. However, for nano-rods with smaller aspect ratios i.e. $w/h = 4$ and 3, laser power affects the stiffness of the rod by decreasing the high strain areas and tailoring the rod stiffness from "weak" to "strong", depending on the applied laser power.

Conclusion

We have presented a molecular dynamics simulation method to print 3D objects voxel by voxel from activated monomers and investigate the structural and mechanical properties of the fabricated 3D polymer networks. Based on the mechanism of free radical polymerization, 3D polymer networks were fabricated from the monomer pool in voxels and the formation of networks is governed by reaction rates constants and defined by classical potential energy functions and types of monomers participating in the elementary reactions. Therefore,

formation of the polymer networks in our method emulates a real polymerization reaction in DLW process and makes it possible to create networks with topologies reminiscent of realistic networks. It has been shown that the degree of monomer conversion and therefore mechanical properties of the polymerized structure can be controlled by changing the laser power and to a lesser extent by changing the writing velocity as long as the exposure time below the threshold value is applied. Furthermore, we found that to fabricate structures with high mechanical properties an optimum writing condition should be applied. While fabricating high aspect ratio structures is desired for many applications, our work highlights the limit in fabricating high aspect ratio structure in DLW, which could not be completely overcome by changing the writing conditions. We showed that the effect of laser power becomes less and less important when the aspect ratio of the printed objects increases.

As experimental methods to observe the 3D printing process on the nanoscale are limited, we believe simulations based on microscopic models can help optimize the printing conditions for smaller and smaller feature sizes. We note that our approach can be expanded for any photoresist to study the effect of writing conditions and architecture on the mechanical properties of polymer networks and may thereby enable substantial reduction of experimental characterizations.

Methods

Polymerization model and algorithm

In the DLW, voxel (volumetic pixel) which is a 3D isosurface of deposited laser intensity in the photoresist, defines the resolution of the two-photon polymerization process. Generally, free-radical polymerization involves at least three steps: initiation, propagation, and termination [59]. In our model, we have used a single bonding algorithm set with appropriate parameters to model radical polymerization and growth of 3D polymer network during the DLW process. The creation of bonds is ruled by the following chemical equation of A (active) and M (monomer)

particles in a given interaction range which react at a rate k and convert to polymerized monomers (T), if they meet criteria explained in the following of the method section.

Initiation: $M \overset{ki}{\rightarrow} A$

Propagation: $A + M \overset{kp}{\rightarrow} T - A$

Branching: $-T - +A \overset{kp}{\rightarrow} \begin{matrix} \vert \\ \mathrm{T}\text{—}\mathrm{A} \\ \vert \end{matrix}$

Crosslinking (and termination): $\begin{matrix} \vert \\ \mathrm{T}\text{—}\mathrm{A} \\ \vert \end{matrix} + \begin{matrix} \vert \\ \mathrm{T}\text{—}\mathrm{A} \\ \vert \end{matrix} \overset{kp}{\rightarrow} \begin{matrix} \vert \\ \mathrm{T}\text{—}\mathrm{T}\text{—}\mathrm{T} \\ \vert \end{matrix}$

Termination by oxygen quenching: $A \overset{kq}{\rightarrow} M\ (T)$

Through initiation reaction the monomer is transformed into active center that can initiate polymerization reactions. In the propagation reaction, the active centers react with monomer molecule to form the first active adduct that is capable of being polymerized. Polymerizations continues in the same manner resulting in the formation of branched macromolecules that are actually end active polymers. The final reaction is termination that can be either by oxygen quenching which deactivates the growth centers or by reaction between two polymers bearing active centers. The described procedure is implemented in our simulations by controlling the monomer type during each elementary reaction and applying respective k for each reaction.

The laser power influences the two-photon absorption and polymerization process by the power of two according to Leatherdale equation for tri-acrylate photoresists [60,61]. Accordingly, in our model the rate of initiation reaction is influenced by the laser power and therefore the “active center” generation rate largely varies for different laser powers. The size of the polymerized voxel is defined by the prolate spheroidal volume being moved three-dimensionally through the box of monomers allowing the fabrication of any 3D polymer network. The *z* axis is taken as the direction of propagation of the laser within the sample. Time evolution of fabrication of

a sample polymer network with pyramidal shape is shown in Fig. 8 and as a movie in the supporting information.

Concentration of monomers and reaction rate constants were derived from experimental data for tri-acrylate based monomers (PETA) photoresist [33]. They are often used in DLW without additional mono or bi-functional monomers for both academic and industrial purposes. The experimental data were converted to probability parameter and are reported in table 1. It should be noted that since each monomer has hydrodynamic radius of about 1 nm according to our calculations, the length scale σ in our model is representative of ~1 nm length.

In the MD simulation of direct laser writing, we use a bead and bead-spring representation of the coarse-grained monomers. The simplest model for an elastomer which can capture the essential features of a rubbery (elastomer) material at the atomic scale is the model developed by Kremer and Grest [62] in which the monomers are lumped together into spherical beads and the beads are connected through elastic springs.

Simulation details

In the MD simulation of direct laser writing, we assume that all the particles in the system have identical masses (m) and interact via a truncated Lennard-Jones 6-12 potential equilibrated as polymer melts at a number density ρ = 0.85 [63]. The ε and σ parameters are the same for all monomers and set to unity in all simulations and the cutoff distance for the bead-bead interactions was set to $r_{cut} = 2.5\sigma$. The connectivity of the network mesh and beads into polymer chains was maintained by the finite extension nonlinear elastic (FENE) potential with the spring constant $k_{spring} = 30\ k_BT/\sigma^2$ and the maximum bond length $R_{max} = 1.5\sigma$ [62]. The repulsive part is represented by truncated-shifted Lennard-Jones (LJ) potential with $r_{cut} = 2^{1/6}\ \sigma$ and $\varepsilon_{LJ} = 1.5k_BT$

$$U_{FENE}(r) = \frac{-1}{2} k_{spring} R_{max}^2 ln\left(1 - \frac{r^2}{R_{max}^2}\right) \qquad (1)$$

This regime is well investigated through previous simulations on different properties of polymeric materials[64–70]. We include some conditions in our simulation in order to control the polymerization reaction. The monomeric units are of functionality three, which means that during polymerization process (resin curing); each active monomer can form up to three bonds with its neighbors. A new bond could be added to an already connected bead as long as the number of bonds per bead is less than the maximum possible number. A monomer could react with an active monomer within a certain probability if the distance of the selected bead is smaller than 1.15σ (reaction radius) from an active monomer. Reactions are performed every Θ MD steps of time step Δt. In all MD simulations for polymer network formation, the NVE ensemble was adopted and periodic boundary conditions were applied on three dimensions. The number of particles in the simulation box varies from ~52000 for one voxel printing to ~1,200,000 for nano-rods that are printed voxel by voxel. All MD runs were performed using the large-scale atomic/ molecular massively parallel simulator (LAMMPS) software developed by Sandia National Laboratories[71]. After fabricating the 3D polymer networks, they were relaxed for at least 5×10^4 τ_{LJ} in NPT ensemble. The temperature is maintained to be constant by coupling the system to a Langevin thermostat [72].

To calculate the Young's modulus, a set of uniaxial tensile deformation were performed to obtain the stress–strain curves. The uniaxial deformation is realized by stepwise stretching the simulation box with $\Delta t=0.01\tau$ along the *x*-axis and at the same time compressing the box along L_z and L_y appropriately to maintain the simulation box being constant. A constant engineering strain rate of $v= 0.0327\tau^{-1}$ was employed during the tensile process which cause the box dimension to change linearly with time in one dimension. It has been shown that the strain rate will affect the stress and hence calculated Young's modulus [73], but since studying this effect is not the purpose of this study, we have used a strain rate which has been used frequently for the similar coarse grained simulations [69,74]. The applied strain rate is comparable with the segmental

relaxation and practical deformation process of elastomers. The tensile stress σ in the *z* direction is calculated from the deviatoric part of the stress tensor[75]:

$$\sigma = (1+\mu)(-P_{zz}+P) = 3\,(-P_{zz}+P)/2 \qquad (2)$$

Where μ is the Poisson's ratio and set to be 0.5 according to the literature and $P = \sum_i P_{ii}/3$ is the hydrostatic pressure [76].

To investigate the influence of aspect ratio of the fabricated polymer network on its mechanical properties, rods with cross section diameters 20σ, 30σ, 40σ and 50σ and 120σ height were prepared by applying laser powers ranging from 10 mW to 50 mW (16 rods). Simulations were performed in a big simulation box 80×80×240 σ (1,200,000 monomers) and rods were printed using 12 layers (voxels) on a substrate consisting of the fixed particles. The exposure time for each voxel were set to be 1200 τ . As the final preparation step, unreacted monomers were removed from the simulation box and the fabricated structures were cooled down at T=0.5 for 50,000 timesteps since equilibration at high temperatures causes flow and a "melting" of the printed structures.

To investigate the stiffness of the printed structures and elucidate how they behave under an external force, we have developed a model to perform bending simulation. To bend the structure, one end of the rod is kept fixed during the simulation, which means that all degrees of freedom are set to zero for the fixed particles. A constant force per particle (F/particle), 0.004 ε/σ is applied in the y direction to the unfixed part of the rods for 5 × 104 τLJ, letting them to exert large deflection as shown in the Fig. 9. The MD simulation of deformation have been performed at T=0.5 and Δτ=0.01 were used. The maximum deflection of each rod (shown in Fig. 9) has been calculated from the average atomic displacement of the particles.

We need a measure that allows us to identify local atomic events within the deformed rods. Falk and Langer [77] developed a method for determining the local deformation of an atomic system by introducing minimum non-affine squared displacement D^2_{min}. Based on the finite-strain

theory, the strain for atom *i* is calculated from the atomic-level deformation gradient and the strain tensor at each particle from the relative motion of its neighbors. Accordingly, atomic strain which is measured using the Green-Lagrangian strain tensor is a good measure of local inelastic deformation [78]. All analysis and calculation of atomic strains and displacements has been performed using OVITO [58].

References

1. Cumpston, B. H. *et al.* Two-photon polymerization initiators for three-dimensional optical data storage and microfabrication. *Nature* **398**, 51–54 (1999).

2. Farsari, M. & Chichkov, B. N. Two-photon fabrication. *Nature Photon* **3**, 450–452 (2009).

3. Deubel, M. *et al.* Direct laser writing of three-dimensional photonic-crystal templates for telecommunications. *Nature Mater* **3**, 444–447 (2004).

4. Zhou, Y. *et al.* Microstructuring of Graphene Oxide Nanosheets Using Direct Laser Writing. *Adv. Mater.* **22**, 67–71 (2010).

5. Grossmann, T. *et al.* Direct laser writing for active and passive high-Q polymer microdisks on silicon. *Opt. Express* **19**, 11451 (2011).

6. Gissibl, T., Thiele, S., Herkommer, A. & Giessen, H. Two-photon direct laser writing of ultracompact multi-lens objectives. *Nature Photon* **10**, 554–560 (2016).

7. LaFratta, C. N., Simoska, O., Pelse, I., Weng, S. & Ingram, M. A convenient direct laser writing system for the creation of microfluidic masters. *Microfluid Nanofluid* **19**, 419–426 (2015).

8. Zeng, H. *et al.* High-Resolution 3D Direct Laser Writing for Liquid-Crystalline Elastomer Microstructures. *Adv. Mater.* **26**, 2319–2322 (2014).

9. Selimis, A., Mironov, V. & Farsari, M. Direct laser writing: Principles and materials for scaffold 3D printing. *Microelectronic Engineering* **132**, 83–89 (2015).

10. Yuk, H. *et al.* 3D printing of conducting polymers. *Nat Commun* **11**, 1604 (2020).

11. Blasco, E. *et al.* Fabrication of Conductive 3D Gold-Containing Microstructures via Direct Laser Writing. *Adv. Mater.* **28**, 3592–3595 (2016).

12. Accardo, A. *et al.* Multiphoton Direct Laser Writing and 3D Imaging of Polymeric Freestanding Architectures for Cell Colonization. *Small* **13**, 1700621 (2017).

13. Hippler, M. *et al.* 3D Scaffolds to Study Basic Cell Biology. *Adv. Mater.* **31**, 1808110 (2019).

14. Bai, Z. *et al.* High-speed laser writing of arbitrary patterns in polar coordinate system. *Review of Scientific Instruments* **87**, 125118 (2016).

15. Jonušauskas, L., Baravykas, T., Andrijec, D., Gadišauskas, T. & Purlys, V. Stitchless support-free 3D printing of free-form micromechanical structures with feature size on-demand. *Sci Rep* **9**, 17533 (2019).

16. Zhang, S.-J. *et al.* Controlling Young's modulus of polymerized structures fabricated by direct laser writing. *Appl. Phys. A* **118**, 437–441 (2015).

17. Lemma, E. D. *et al.* Mechanical properties tunability of three-dimensional polymeric structures in two-photon lithography. *IEEE Trans. Nanotechnology* 1–1 (2016) doi:10.1109/TNANO.2016.2625820.

18. Sakellari, I. *et al.* Diffusion-Assisted High-Resolution Direct Femtosecond Laser Writing. *ACS Nano* **6**, 2302–2311 (2012).

19. Fischer, J. & Wegener, M. Three-dimensional direct laser writing inspired by stimulated-emission-depletion microscopy [Invited]. *Opt. Mater. Express* **1**, 614 (2011).

20. Wang, S. *et al.* Sub-10-nm suspended nano-web formation by direct laser writing. *Nano Futures* **2**, 025006 (2018).

21. He, P. J. W., Katis, I. N., Eason, R. W. & Sones, C. L. Laser direct-write for fabrication of three-dimensional paper-based devices. *Lab Chip* **16**, 3296–3303 (2016).

22. Wang, W. *et al.* Direct Laser Writing of Superhydrophobic PDMS Elastomers for Controllable Manipulation via Marangoni Effect. *Adv. Funct. Mater.* **27**, 1702946 (2017).

23. Sharma, R. *et al.* Fabrication of Functional Nanophotonic Devices via Multiphoton Polymerization. in *ACS Symposium Series* (eds. Seppala, J. E., Kotula, A. P. & Snyder, C. R.) vol. 1315 151–171 (American Chemical Society, 2019).

24. Greiner, A. M. *et al.* Multifunctional polymer scaffolds with adjustable pore size and chemoattractant gradients for studying cell matrix invasion. *Biomaterials* **35**, 611–619 (2014).

25. Ovsianikov, A. *et al.* Shrinkage of microstructures produced by two-photon polymerization of Zr-based hybrid photosensitive materials. *Opt. Express* **17**, 2143 (2009).

26. Rekštytė, S., Paipulas, D., Malinauskas, M. & Mizeikis, V. Microactuation and sensing using reversible deformations of laser-written polymeric structures. *Nanotechnology* **28**, 124001 (2017).

27. Varapnickas, S. & Malinauskas, M. *Processes of Direct Laser Writing 3D Nano-Lithography*. http://www.preprints.org/manuscript/201812.0119/v1 (2018) doi:10.20944/preprints201812.0119.v1.

28. Bauer, J., Guell Izard, A., Zhang, Y., Baldacchini, T. & Valdevit, L. Programmable Mechanical Properties of Two-Photon Polymerized Materials: From Nanowires to Bulk. *Adv. Mater. Technol.* **4**, 1900146 (2019).

29. Bartolo, P. J. & Lenz, E. Computer simulation of stereolithographic curing reactions: phenomenological versus mechanistic approaches. *CIRP Annals* **55**, 221–225 (2006).

30. Baschnagel, J., Wittmer, J. P. & Meyer, H. Monte Carlo SImulation of Polymers: Coarse-Grained Models. *arXiv:cond-mat/0407717* (2004).

31. Perry, M. F. & Young, G. W. A Mathematical Model for Photopolymerization From a Stationary Laser Light Source. *Macromol. Theory Simul.* **14**, 26–39 (2005).

32. Uppal, N. Modeling of temperature-dependent diffusion and polymerization kinetics and their effects on two-photon polymerization dynamics. *J. Micro/Nanolith. MEMS MOEMS* **7**, 043002 (2008).

33. Mueller, J. B., Fischer, J., Mayer, F., Kadic, M. & Wegener, M. Polymerization Kinetics in Three-Dimensional Direct Laser Writing. *Adv. Mater.* **26**, 6566–6571 (2014).

34. Landman, U. & Luedtke, W. D. Small is different: energetic, structural, thermal, and mechanical properties of passivated nanocluster assemblies. *Faraday Disc.* **125**, 1 (2004).

35. Tan, J. C. & Cheetham, A. K. Mechanical properties of hybrid inorganic–organic framework materials: establishing fundamental structure–property relationships. *Chem. Soc. Rev.* **40**, 1059 (2011).

36. Matveeva, A. Y., Pyrlin, S. V., Ramos, M. M. D., Böhm, H. J. & van Hattum, F. W. J. Influence of waviness and curliness of fibres on mechanical properties of composites. *Computational Materials Science* **87**, 1–11 (2014).

37. Liu, J. *et al.* Formation mechanism of bound rubber in elastomer nanocomposites: a molecular dynamics simulation study. *RSC Adv.* **8**, 13008–13017 (2018).

38. Shao, J. *et al.* Monte Carlo simulation on kinetics of batch and semi-batch free radical polymerization. *Macromol. Res.* **23**, 1042–1050 (2015).

39. Komarov, P. V., Yu-Tsung, C., Shih-Ming, C., Khalatur, P. G. & Reineker, P. Highly Cross-Linked Epoxy Resins: An Atomistic Molecular Dynamics Simulation Combined with a Mapping/Reverse Mapping Procedure. *Macromolecules* **40**, 8104–8113 (2007).

40. Wang, Z., Liang, H. & Dobrynin, A. V. Computer Simulations of Continuous 3-D Printing. *Macromolecules* **50**, 7794–7800 (2017).

41. Baldacchini, T., Zimmerley, M., Kuo, C.-H., Potma, E. O. & Zadoyan, R. Characterization of Microstructures Fabricated by Two-Photon Polymerization Using Coherent Anti-Stokes Raman Scattering Microscopy. *J. Phys. Chem. B* **113**, 12663–12668 (2009).

42. Cicha, K. *et al.* Evaluation of 3D structures fabricated with two-photon-photopolymerization by using FTIR spectroscopy. *Journal of Applied Physics* **110**, 064911 (2011).

43. Jiang, L. J. *et al.* Two-photon polymerization: investigation of chemical and mechanical properties of resins using Raman microspectroscopy. *Opt. Lett.* **39**, 3034 (2014).

44. Ziemke, P., Frenzel, T., Wegener, M. & Gumbsch, P. Tailoring the characteristic length scale of 3D chiral mechanical metamaterials. *Extreme Mechanics Letters* **32**, 100553 (2019).

45. Gernhardt, M. *et al.* Tailoring the Mechanical Properties of 3D Microstructures Using Visible Light Post-Manufacturing. *Adv. Mater.* 1901269 (2019) doi:10.1002/adma.201901269.

46. Hahn, V. *et al.* Rapid Assembly of Small Materials Building Blocks (Voxels) into Large Functional 3D Metamaterials. *Adv. Funct. Mater.* **30**, 1907795 (2020).

47. Voyiadjis, G. Z. & Kattan, P. I. Advances in the mechanics of undamageable materials: General three-dimensional formulation. *International Journal of Damage Mechanics* **28**, 1021–1037 (2019).

48. Fischer, J. & Wegener, M. Three-dimensional optical laser lithography beyond the diffraction limit: 3D optical lithography off limits. *Laser & Photonics Reviews* **7**, 22–44 (2013).

49. Stevens, M. M. Exploring and Engineering the Cell Surface Interface. *Science* **310**, 1135–1138 (2005).

50. Bougdid, Y. *et al.* Systematic λ /21 resolution achieved in nanofabrication by two-photon-absorption induced polymerization. *J. Micromech. Microeng.* **29**, 035018 (2019).

51. Melissinaki, V. *et al.* Direct laser writing of 3D scaffolds for neural tissue engineering applications. *Biofabrication* **3**, 045005 (2011).

52. Fischer, J. *et al.* Three-dimensional multi-photon direct laser writing with variable repetition rate. *Opt. Express* **21**, 26244 (2013).

53. Mohamed, K. & M., M. The Fabrication of High Aspect Ratio Nanostructures on Quartz Substrate. in *Updates in Advanced Lithography* (ed. Hosaka, S.) (InTech, 2013). doi:10.5772/56315.

54. Jeon, H.-J., Kim, K. H., Baek, Y.-K., Kim, D. W. & Jung, H.-T. New Top-Down Approach for Fabricating High-Aspect-Ratio Complex Nanostructures with 10 nm Scale Features. *Nano Lett.* **10**, 3604–3610 (2010).

55. Frenzel, T., Kadic, M. & Wegener, M. Three-dimensional mechanical metamaterials with a twist. *Science* **358**, 1072–1074 (2017).

56. Bückmann, T. *et al.* Tailored 3D Mechanical Metamaterials Made by Dip-in Direct-Laser-Writing Optical Lithography. *Adv. Mater.* **24**, 2710–2714 (2012).

57. Kang, K., Cho, Y. & Yu, K. Novel Nano-Materials and Nano-Fabrication Techniques for Flexible Electronic Systems. *Micromachines* **9**, 263 (2018).

58. Stukowski, A. Visualization and analysis of atomistic simulation data with OVITO–the Open Visualization Tool. *Modelling Simul. Mater. Sci. Eng.* **18**, 015012 (2010).

59. Moad, G. Radical Polymerization. in *Reference Module in Materials Science and Materials Engineering* B9780128035818013000 (Elsevier, 2016). doi:10.1016/B978-0-12-803581-8.01346-1.

60. Leatherdale, C. A. & DeVoe, R. J. Two-photon microfabrication using two-component photoinitiation systems: effect of photosensitizer and acceptor concentrations. in (eds. Yeates, A. T., Belfield, K. D., Kajzar, F. & Lawson, C. M.) 112 (2003). doi:10.1117/12.508087.

61. DeVoe, R. J., Kalweit, H. W., Leatherdale, C. A. & Williams, T. R. Voxel shapes in two-photon microfabrication. in (eds. Belfield, K. D., Caracci, S. J., Kajzar, F., Lawson, C. M. & Yeates, A. T.) 310 (2003). doi:10.1117/12.459028.

62. Kremer, K. & Grest, G. S. Dynamics of entangled linear polymer melts: A molecular-dynamics simulation. *The Journal of Chemical Physics* **92**, 5057–5086 (1990).

63. *Understanding Molecular Simulation*. (Elsevier, 2002). doi:10.1016/B978-0-12-267351-1.X5000-7.

64. Liang, H., Wang, Z. & Dobrynin, A. V. Scattering from Melts of Combs and Bottlebrushes: Molecular Dynamics Simulations and Theoretical Study. *Macromolecules* **52**, 5555–5562 (2019).

65. Liang, H., Cao, Z., Wang, Z. & Dobrynin, A. V. Surface Stress and Surface Tension in Polymeric Networks. *ACS Macro Lett.* **7**, 116–121 (2018).

66. Sayko, R., Wang, Z., Liang, H., Becker, M. L. & Dobrynin, A. V. Degradation of Films of Block Copolymers: Molecular Dynamics Simulations. *Macromolecules* **53**, 1270–1280 (2020).

67. Liang, H., Wang, Z. & Dobrynin, A. V. Strain-Adaptive Self-Assembled Networks of Linear-Bottlebrush-Linear Copolymers. *Macromolecules* **52**, 8617–8624 (2019).

68. Wang, Z., Liang, H., Adamson, D. H. & Dobrynin, A. V. From Graphene-like Sheet Stabilized Emulsions to Composite Polymeric Foams: Molecular Dynamics Simulations. *Macromolecules* **51**, 7360–7367 (2018).

69. Wei, M. *et al.* Molecular dynamics simulation on the mechanical properties of natural-rubber- *graft* -rigid-polymer/rigid-polymer systems. *Phys. Chem. Chem. Phys.* **20**, 8228–8240 (2018).

70. Paturej, J., Sheiko, S. S., Panyukov, S. & Rubinstein, M. Molecular structure of bottlebrush polymers in melts. *Sci. Adv.* **2**, e1601478 (2016).

71. Plimpton, S. Fast Parallel Algorithms for Short-Range Molecular Dynamics. *Journal of Computational Physics* **117**, 1–19 (1995).

72. Davidchack, R. L., Handel, R. & Tretyakov, M. V. Langevin thermostat for rigid body dynamics. *The Journal of Chemical Physics* **130**, 234101 (2009).

73. Sahputra, I. H. & Echtermeyer, A. T. Effects of temperature and strain rate on the deformation of amorphous polyethylene: a comparison between molecular dynamics simulations and experimental results. *Modelling Simul. Mater. Sci. Eng.* **21**, 065016 (2013).

74. Gao, J. & Weiner, J. H. Simulated polymer melt stress relaxation. I. Plateau behavior. *The Journal of Chemical Physics* **103**, 1614–1620 (1995).

75. Wang, L. *et al.* Stress–strain behavior of block-copolymers and their nanocomposites filled with uniform or Janus nanoparticles under shear: a molecular dynamics simulation. *Phys. Chem. Chem. Phys.* **18**, 27232–27244 (2016).

76. Liu, J., Wu, S., Zhang, L., Wang, W. & Cao, D. Molecular dynamics simulation for insight into microscopic mechanism of polymer reinforcement. *Phys. Chem. Chem. Phys.* **13**, 518–529 (2011).

77. Falk, M. L. & Langer, J. S. Dynamics of viscoplastic deformation in amorphous solids. *Phys. Rev. E* **57**, 7192–7205 (1998).

78. Shimizu, F., Ogata, S. & Li, J. Theory of Shear Banding in Metallic Glasses and Molecular Dynamics Calculations. *Mater. Trans.* **48**, 2923–2927 (2007).

Acknowledgments

The authors thank Dr. Zilu Wang from Akron University for valuable discussions on polymerization simulation techniques. We also thanks Prof. Eva Blasco, Prof. Martin Wegener and Pascal Kiefer for fruitful discussion on 3D printing techniques. This research was funded by the Deutsche Forschungsgemeinschaft (DFG, German Research Foundation) under Germany's Excellence Strategy via the Excellence Cluster 3D Matter Made to Order (EXC-2082/1-390761711), by the Carl Zeiss Foundation through the "Carl-Zeiss-Focus@HEiKA,"by the Helmholtz program "Science and Technology of Nanosystems".

Funding: Deutsche Forschungsgemeinschaft (2082/1 – 390761711); Carl-Zeiss-Stiftung and Open Access Publishing Fund of Karlsruhe Institute of Technology

Author contributions: W.W. and E.S. conceived the study. E.S. and M.L. developed the model and performed the simulations and analysis. E.S. wrote the manuscript. Supervision, project administration and funding acquisition were done by W.W. All authors edited the manuscript and approved its final version.

Competing interests: The authors declare no competing interests.

Data and materials availability: All data needed to evaluate the conclusions in the paper are present in the paper and/or the Supplementary Materials.

Figures and Tables

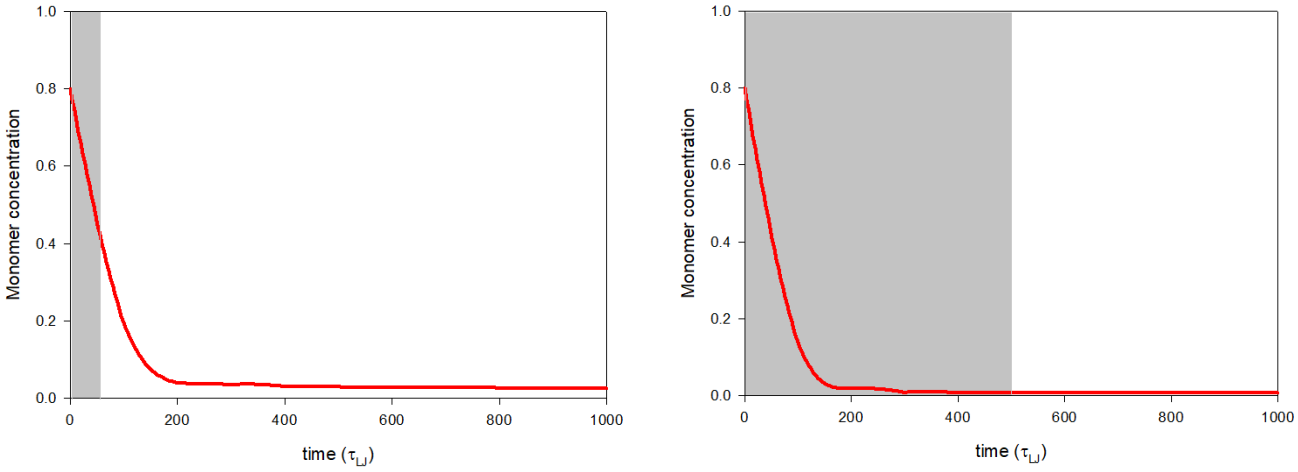

Fig. 1. Kinetics of monomer consumption for two exposure times (50 and 500 τ). The gray areas show exposure times.

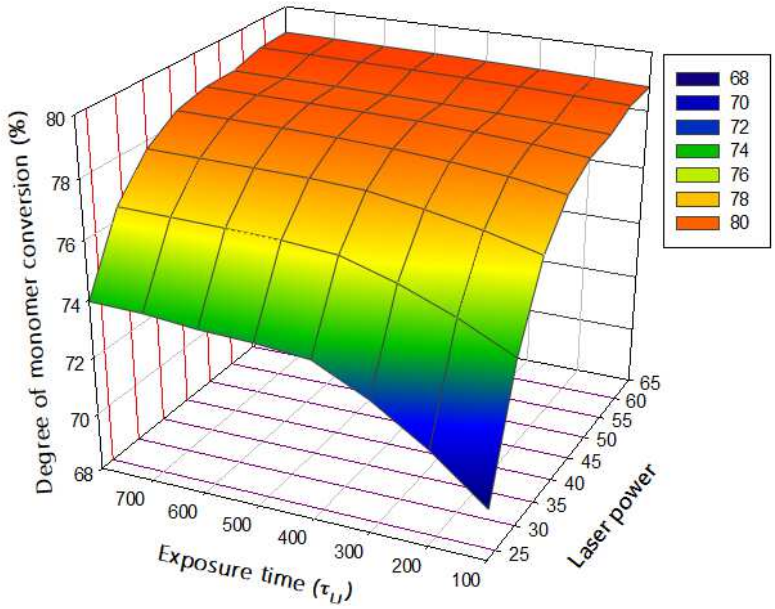

Fig.2. Degree of monomer conversion with respect to exposure time and laser power.

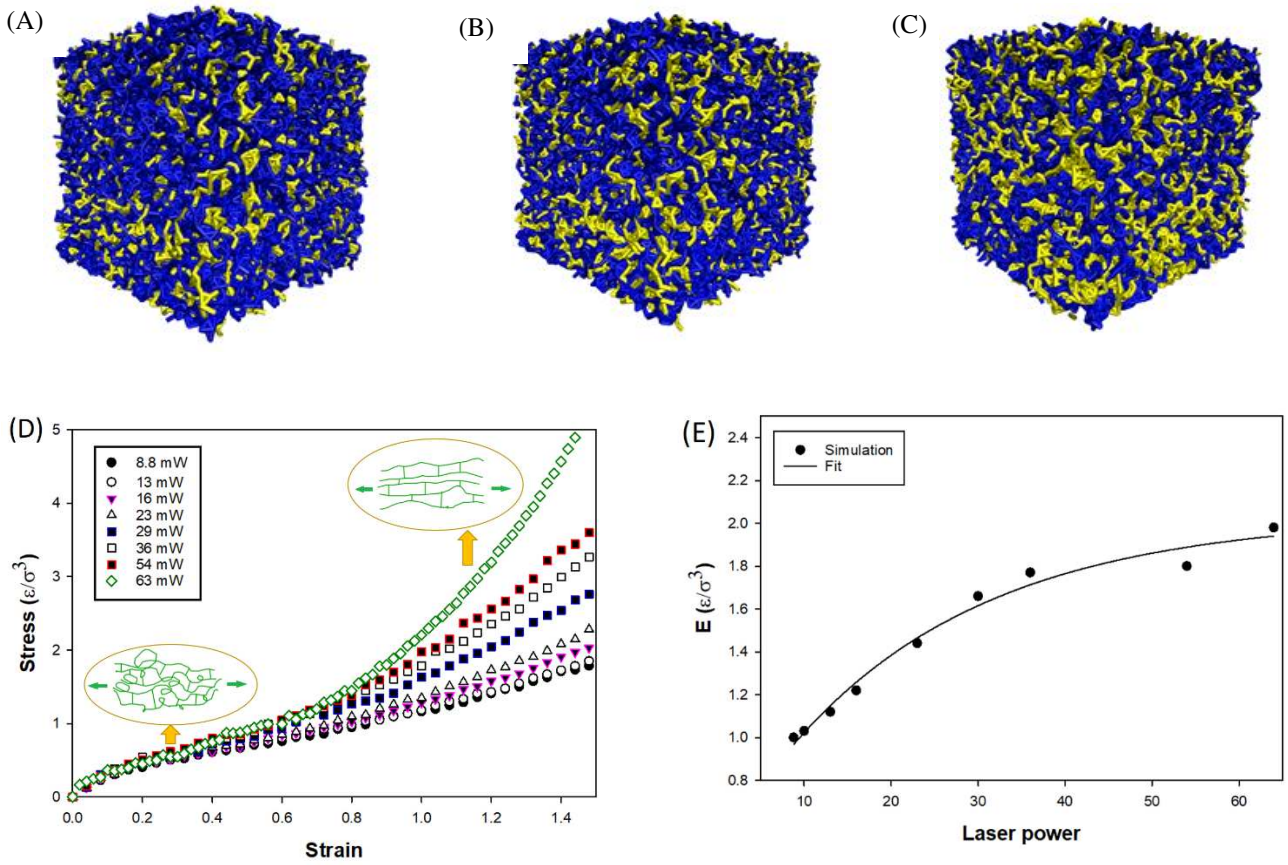

Fig. 3. (A-C) 3D polymer blocks printed applying different laser powers, yellow regions represents cross linked monomers illustrate the increase in the cross-linking density as the laser power increases (D) Stress-strain curve for the printed networks with different laser powers (E) calculated young modulus as a function of the laser power.

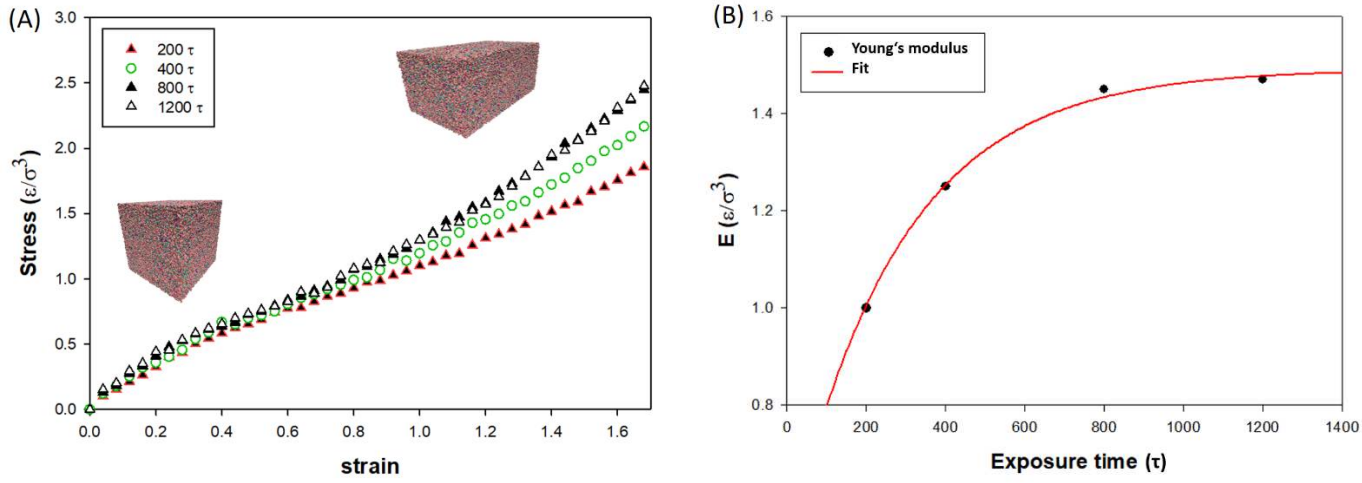

Fig. 4. (A) Stress-strain curve for printed blocks applying different exposure times (B) Young's modulus calculated from the slopes of the stress-strain curve.

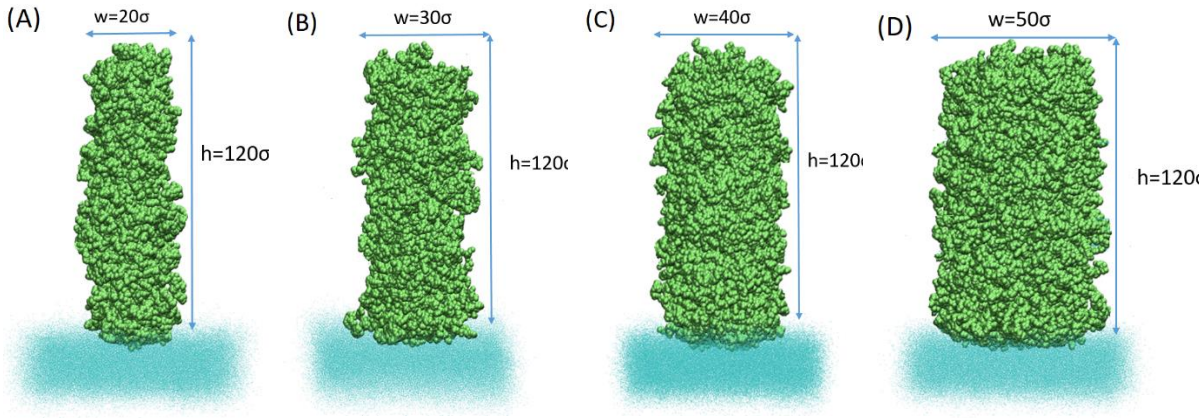

Fig. 5. Printed rods with different aspect ratios, (A) h/w=6 (B) h/w=4w= (C) h/w=3w= and (D) wh/w=2.4

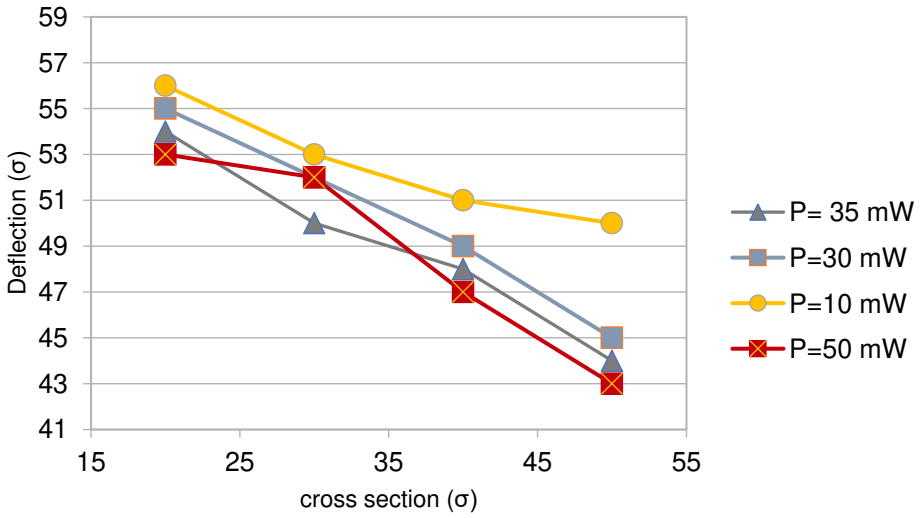

Fig. 6. Maximum deflection of the printed rods vs. cross section diameter for different laser powers

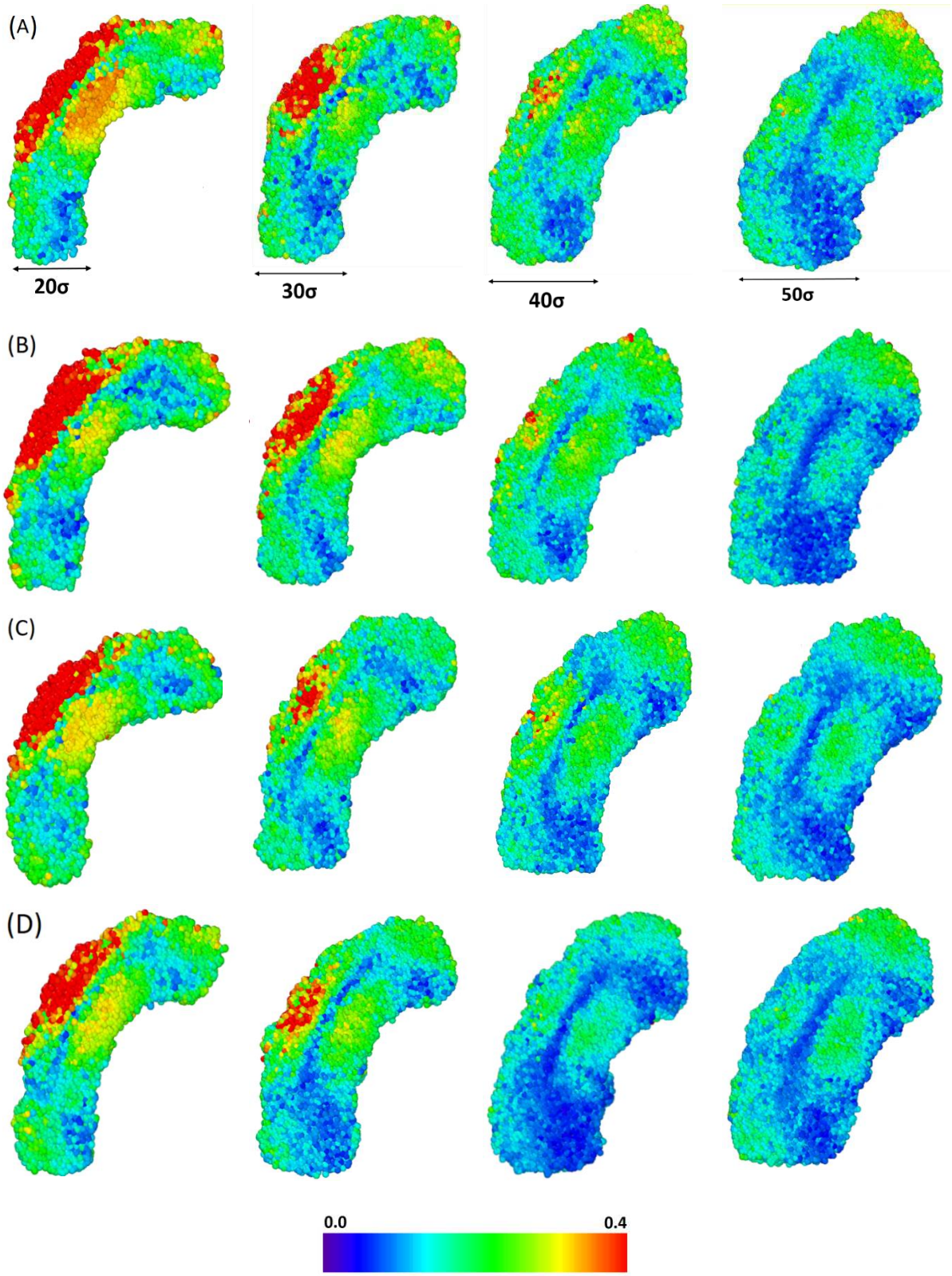

Fig. 7. Distribution of atomic strain in printed rods of different aspect ratios with atoms colored according to their strain for laser power. (A) 10 mW (B) 30 mW (C) 35 mW and (D) 50 mW. Color map is for atomic strain and the rods are sliced through the slab centers.

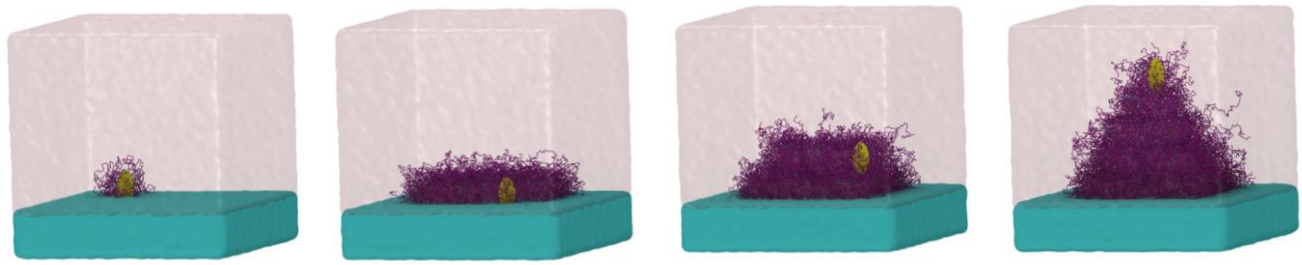

Fig. 8. Time evolution of the pyramid growth during direct laser writing. The yellow volume represents the laser exposure area (voxel). The pink glassy area represents the unreacted monomers.

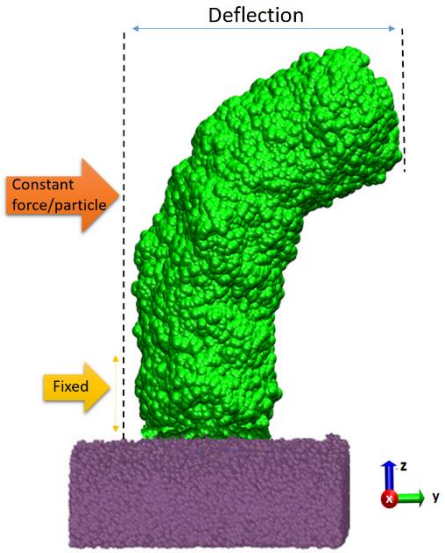

Fig. 9. Schematic presentation of rod deformation by external applied force.

Table 1. Parameters that are used in the simulations to control laser writing condition and polymerization reactions [33].

Parameters	**Value**	**Description**
A, M, T	-	Types of reacting (A) and resulting (M,T) CG beads
$P_{polymerization}$	0.74	The probability with which polymerization happens
$P_{quenching}$	0.26	The probability with which active monomers deactivate (oxygen quenching)
[ρ]	0.85	Number density of the monomers in the simulation box
P_{laser}	αP^2 P=laser power and α=0.007	The probability with which active monomers are generated
E	Simulation time	Exposure time (τ_{LJ})
τ_R	10	Time intervals between two reactive MD steps

Supplementary Materials

Movies S1. Fabrication of a pyramid polymer network in a cubic monomer pool. Free monomers are shown in a pink glassy material.

Movie S2. Fabrication of a rod in a cubic monomer pool.

Figures

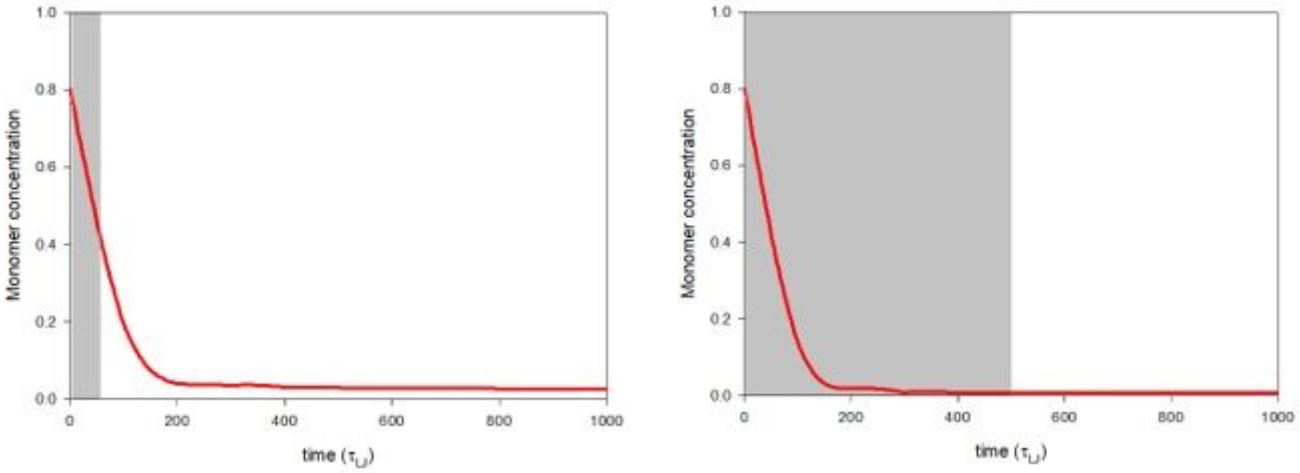

Figure 1

Kinetics of monomer consumption for two exposure times (50 and 500 τ). The gray areas show exposure times.

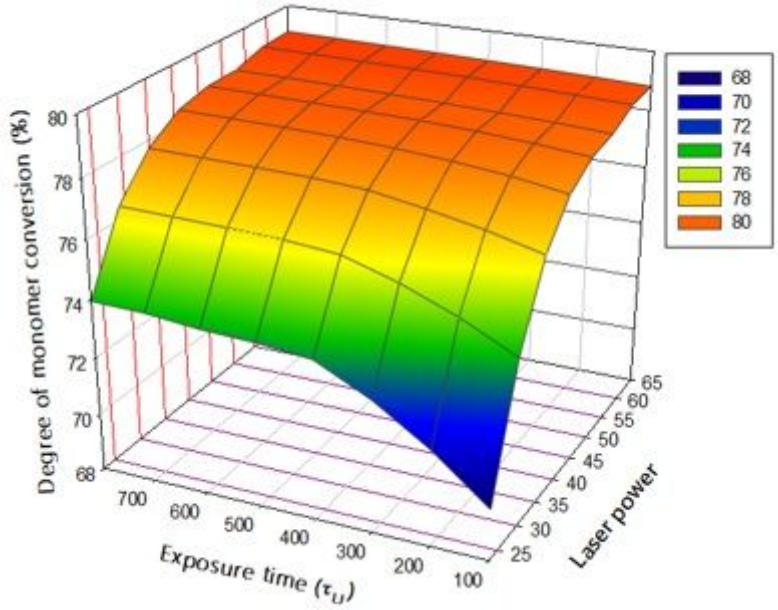

Figure 2

Degree of monomer conversion with respect to exposure time and laser power.

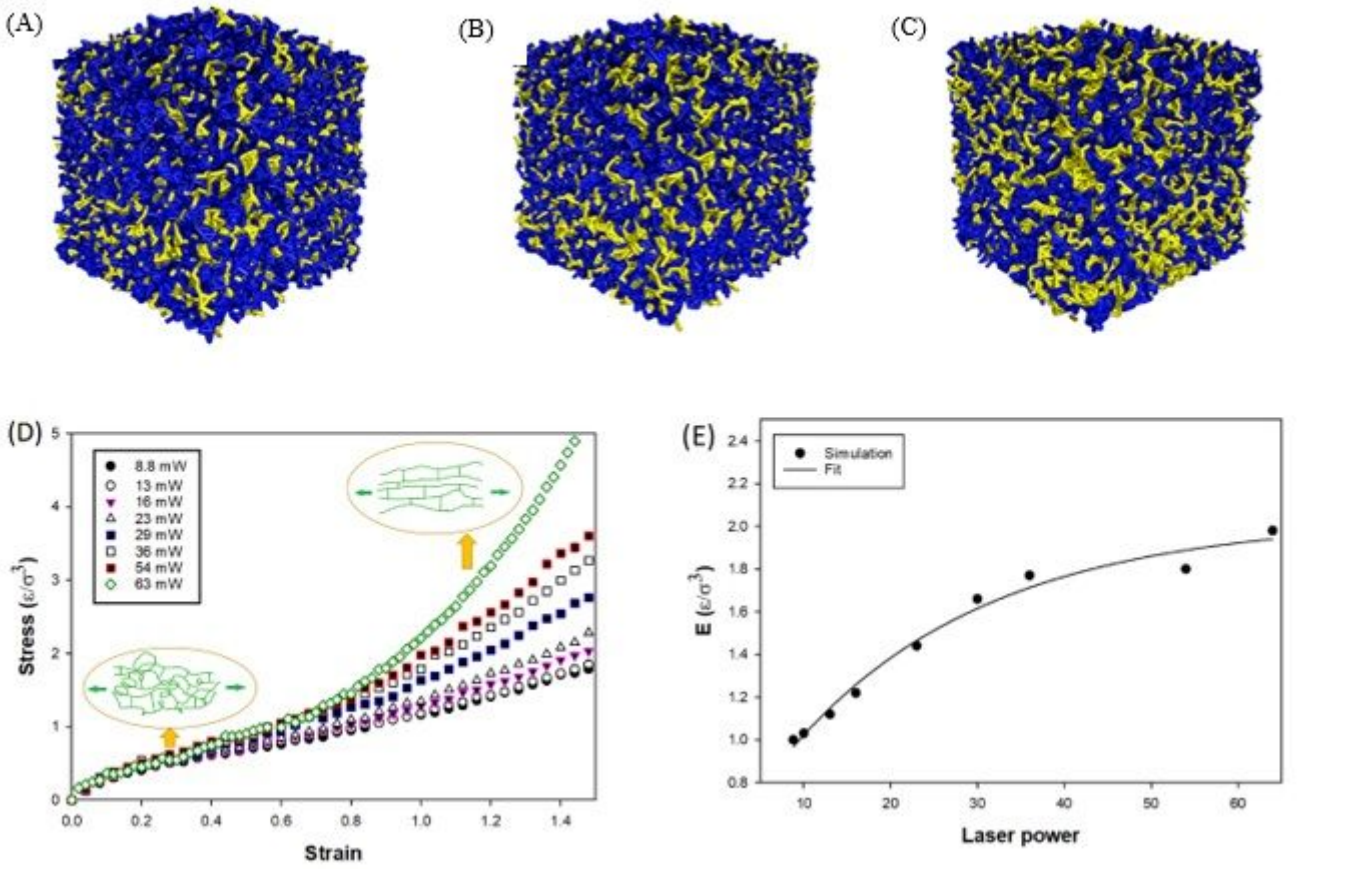

Figure 3

(A-C) 3D polymer blocks printed applying different laser powers, yellow regions represents cross linked monomers illustrate the increase in the cross-linking density as the laser power increases (D) Stress-strain curve for the printed networks with different laser powers (E) calculated young modulus as a function of the laser power.

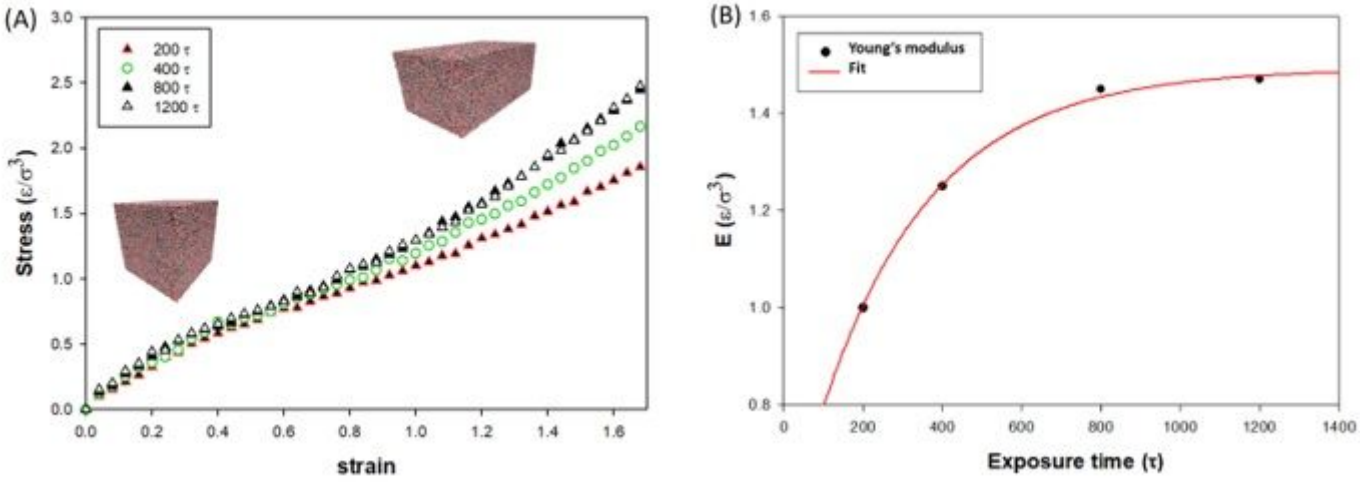

Figure 4

(A) Stress-strain curve for printed blocks applying different exposure times (B) Young's modulus calculated from the slopes of the stress-strain curve.

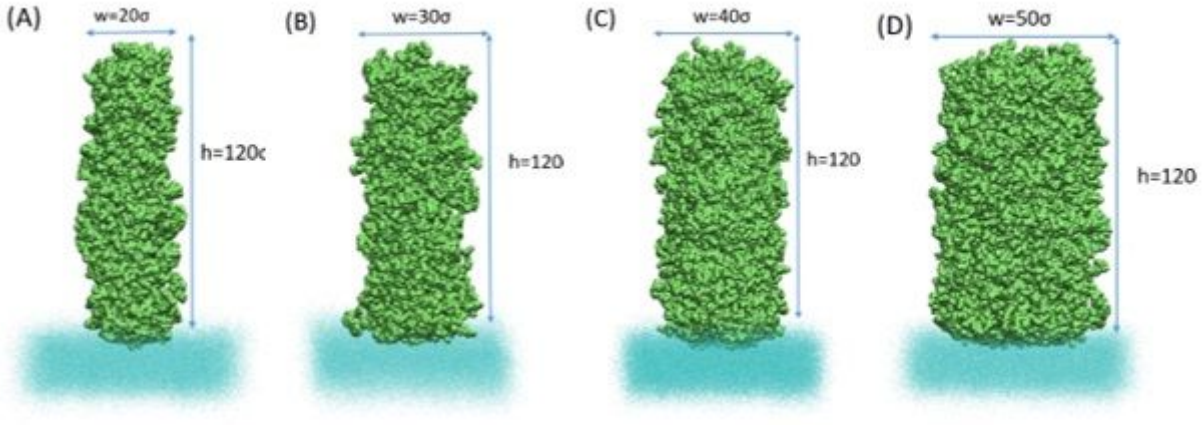

Figure 5

Printed rods with different aspect ratios, (A) h/w=6 (B) h/w=4w= (C) h/w=3w= and (D) wh/w=2.4

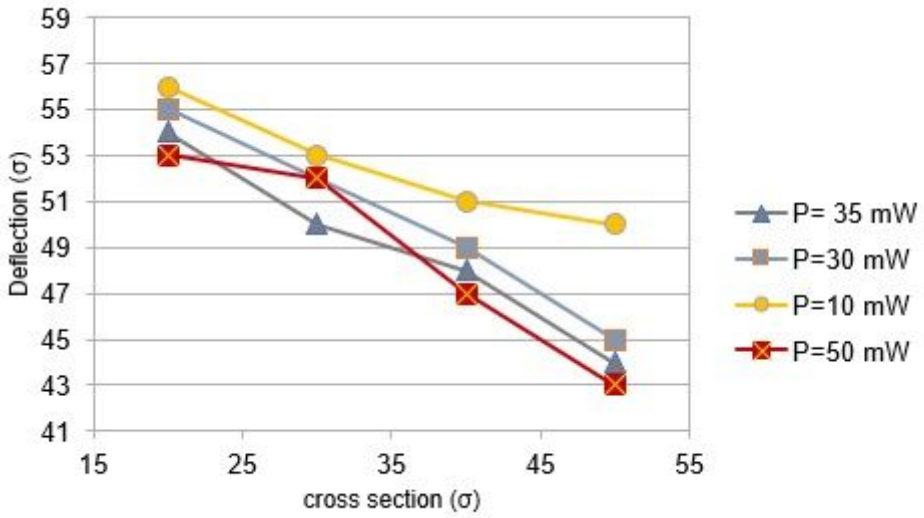

Figure 6

Maximum deflection of the printed rods vs. cross section diameter for different laser powers

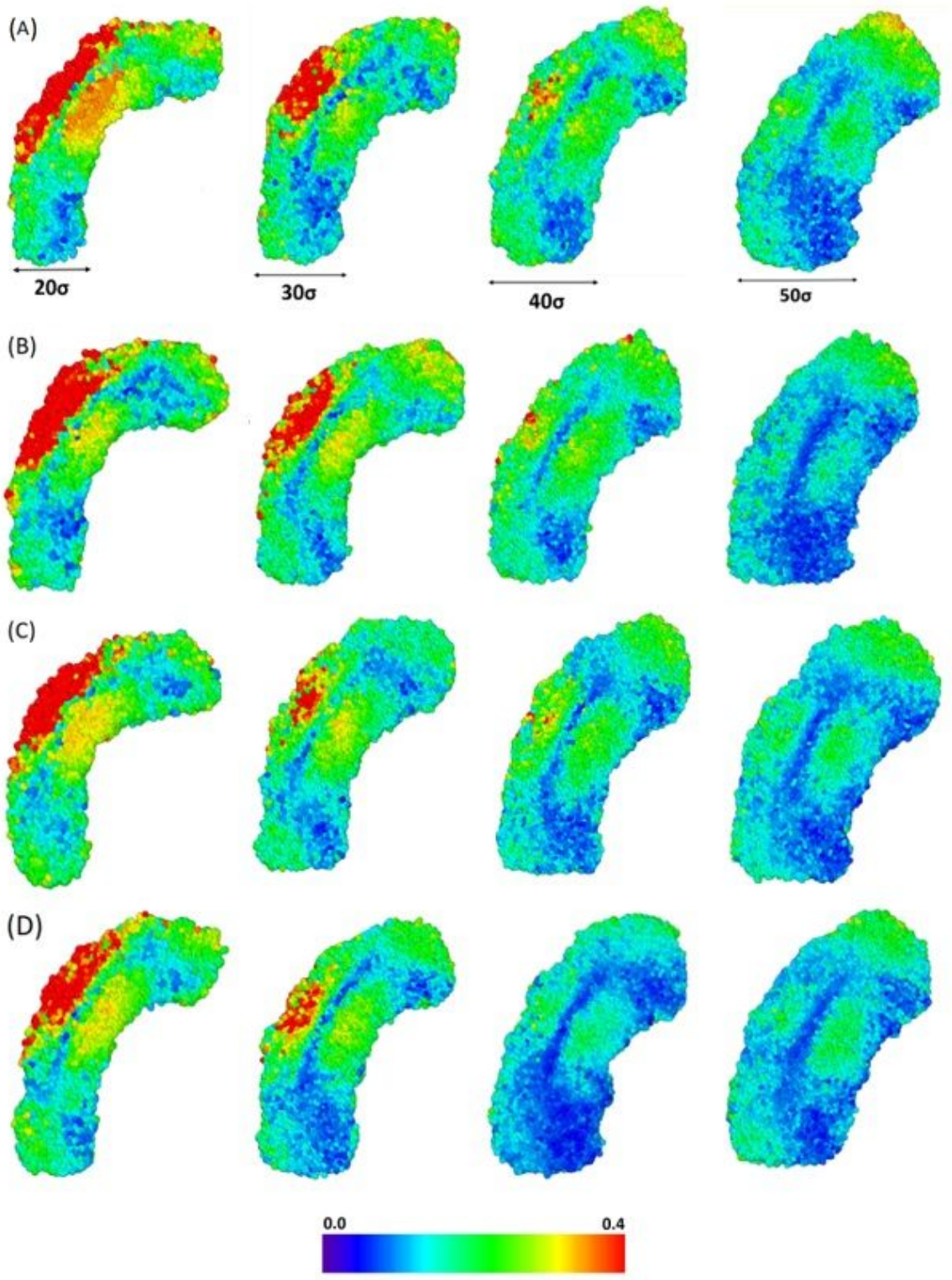

Figure 7

Distribution of atomic strain in printed rods of different aspect ratios with atoms colored according to their strain for laser power. (A) 10 mW (B) 30 mW (C) 35 mW and (D) 50 mW. Color map is for atomic strain and the rods are sliced through the slab centers.

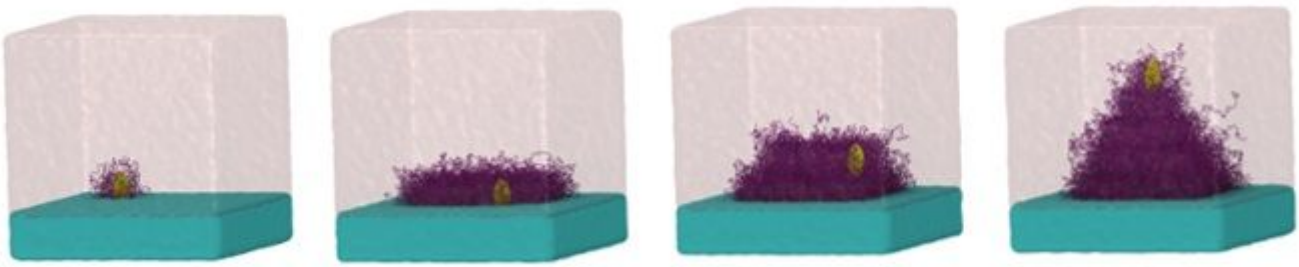

Figure 8

Time evolution of the pyramid growth during direct laser writing. The yellow volume represents the laser exposure area (voxel). The pink glassy area represents the unreacted monomers.

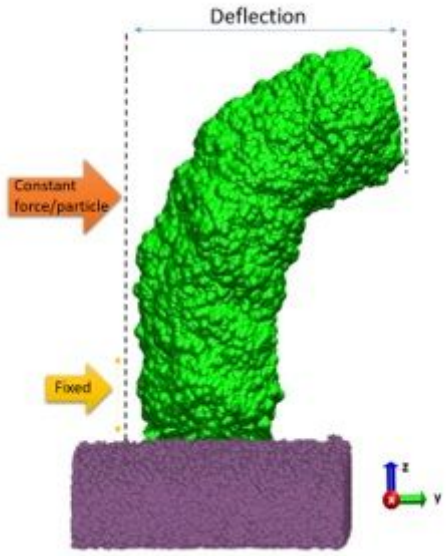

Figure 9

Schematic presentation of rod deformation by external applied force.

Supplementary Files

This is a list of supplementary files associated with this preprint. Click to download.

- movieS1.mp4
- movieS2.mp4